Detection of Scab-Damaged Hard Red Spring Wheat Kernels by Near-Infrared Reflectance

Stephen R. Delwiche[1,2] and Gary A. Hareland[3]

ABSTRACT

Cereal Chem. 81(5):643–649

Scab (Fusarium head blight) is a fungal disease that has become increasingly prevalent in North American wheat during the past 15 years. It is of concern to growers, processors, and the consumers because of depressed yields, poor flour quality, and the potential for elevated concentrations of the mycotoxin, deoxynivalenol (DON). Both wheat breeder and wheat inspector must currently deal with the assessment of scab in harvested wheat by manual human inspection. The study described herein examined the accuracy of a semi-automated wheat scab inspection system that is based on near-infrared (NIR) reflectance (1,000–1,700 nm) of individual kernels. Using statistical classification techniques such as linear discriminant analysis and nonparametric (*k*-nearest-neighbor) classification, upper limits of accuracy for NIR-based classification schemes of ≈88% (cross-validation) and 97% (test) were determined. An exhaustive search of the most suitable wavelength pairs for the spectral difference, $[\log(1/R)_{\lambda 1} - \log(1/R)_{\lambda 2}]$, revealed that the slope of the low-wavelength side of a broad carbohydrate absorption band (centered at ≈1,200 nm) was very effective at discriminating between healthy and scab-damaged kernels with test set accuracies of 95%. The achieved accuracy levels demonstrate the potential for the use of NIR spectroscopy in commercial sorting and inspection operations for wheat scab.

Fusarium head blight, also known as scab, is a fungal disease that affects wheat and other cereals. Primarily caused by *F. graminearum*, scab occurs during the flowering and early kernel development stages of the plant under conditions of rain and elevated humidities. Depending on the year, hard red spring wheats of the Northern Great Plains of the United States and western prairie provinces of Canada are susceptible to scab (such as in 1993), as are the soft red winter wheat growing regions in the eastern United States, particularly in 1996 and 2003. Infection with *Fusarium* results in depressed yields caused by kernels that are either too light in mass for mechanized harvesting (Bai and Shaner 1994) or low in test weight (Cunfer 1987; Dexter et al 1996). Scab infection may also have a deleterious effect on flour color, ash content, and baking performance (Dexter et al 1996), with these and other quality issues recently reviewed by Dexter and Nowicki (2003). Also considered as a component in a category collectively called damaged in federal official inspection, wheat lots >2% damaged kernels by weight are progressively downgraded from the U.S. No. 1 grade (USDA-GIPSA 1997). Grade is reduced (to No. 5) with increased levels of damaged kernels until the weight concentration reaches 15%, whereupon a lot is assigned the grade of sample grade. Often, domestic processors and overseas buyers have even more stringent criteria for percentages of scab-damaged kernels.

Beyond that of physical damage to the kernel, *F. graminearum* can produce the metabolite, deoxynivalenol (DON), or vomitoxin, a tricothecene mycotoxin that is a health concern. The U.S. Food and Drug Administration (FDA) has established an advisory level for DON in finished wheat products (e.g., flour, semolina) intended for human consumption at 1 ppm, and at higher levels (5–10 ppm) for livestock and poultry feeds. Teich et al (1987) measured a positive correlation between the levels of DON and scab damage. Therefore, as a means to improve the quality and safety of wheat in the United States, the USDA is currently seeking new methods for grain inspection, inclusive of those that address kernel damage (e.g., scab) that are rapid and objectively based.

Numerous procedures are available for measurement of DON level concentration in wheat meal and flour, including those based on thin-layer chromatography (Truckness et al 1984; Fernandez et al 1994), liquid chromatography (Chang et al 1984; Trenholm et al 1985; Rajaklyä et al 1987), gas chromatography (GC) (Terhune et al 1984; Ware et al 1984; Scott et al 1986; Tacke et al 1996), GC with mass spectrometry (Scott et al 1981), and enzyme-linked immunosorbent assay (ELISA) (Casale et al 1988; Usleber et al 1991, 1993; Abramson et al 1998). However, these procedures are not adaptable to rapid (<1 min/sample) testing for inspection or process control.

Rapid inspection or sorting methods for grain are typically based on kernel density (Tkachuk et al 1991) or optical properties (Ruan et al 1998). Preliminary research by Williams (1997) demonstrated moderate success with the NIR modeling of DON in bulk samples. Recent work by Pettersson and Åberg (2003) on scab-damaged wheat prepared by dilution series has also indicated the potential of DON level by whole grain NIR transmittance. At the single kernel level, Dowell et al (1999) examined the ability of NIR reflectance to measure DON concentration. Using a similar approach to that described herein on a limited set of officially inspected wheat, we demonstrated the ability to distinguish normal, mold-damaged, and scab-damaged categories (Delwiche 2003). Based on a more diverse collection of hard red spring wheat samples, the research described herein was directed at identifying regions within the near-infrared (NIR) region of 1,000–1,700 nm that can be used, with or without kernel mass, to determine the extent of scab-damage within wheat samples through single kernel inspection. Specifically, the objective of this study was to identify and characterize a pair of wavelengths for an NIR reflectance system that can form the basis of a commercial sorting device or inspection instrument.

MATERIALS AND METHODS

Wheat. Hard red spring wheat samples were obtained from two distinct breeders' trials. The first trial consisted of the 37 lines that were the basis for the Hard Red Spring Uniform Regional Nursery (HRS-URN) trial set for the 2002 harvest. Of the 37 lines, five were commercial releases (cultivars Marquis, Chris, 2375, Verde, and Keene); the remaining were breeders' advanced lines. All lines were grown in field plots under conventional growing practices at two geographical locations, Crookston and St. Paul, MN. The second trial consisted of a breeder's advanced

[1] USDA/ARS, Beltsville Agricultural Research Center, Instrumentation and Sensing Laboratory, Building 303, BARC-East, Beltsville, MD 20705-2350. Names are necessary to report factually on available data; however, the USDA neither guarantees nor warrants the standard of the product, and the use of the name by the USDA implies no approval of the product to the exclusion of others that may also be suitable.
[2] Corresponding author. E-mail: delwiche@ba.ars.usda.gov
[3] USDA/ARS, Hard Red Spring and Durum Wheat Quality Laboratory, Fargo, ND.

Publication no. C-2004-0805-02R.

yield (AY) set, in which 45 lines from seven commercial releases (Oxen, Alsen, Verde, Bacup, Roblin, McVey, and Wheaton) were grown in the 2002 harvest in two replicates in randomized complete blocks at the same locations as the first trial. One replicate from St. Paul was unavailable. Wheat plants of the AY St. Paul samples were inoculated with *Fusarium* by conidia spraying at the heading stage. The AY Crookston plants were also inoculated with *Fusarium*, however, the inoculation was performed by spreading corn kernels that had been infected with 10 strains of naturally occurring *Fusarium* onto the developing wheat plants at the jointing stage.

Equipment. The NIR (943.3–1,704.6 nm) spectrometer assembly was described earlier (Delwiche 2003). Briefly, it consisted of a Zeiss MCS511 (Jena, Germany) diode array bench unit operating within the Grams/32 (Galactic Industries, Salem, NH) software environment. Lighting was supplied by two externally controlled 5V, 150 mA tungsten filament lamps with gold-coated parabolic reflectors. Reflectance energy values were referenced to sintered polytetrafluoroethylene (Spectralon, Labsphere, Sutton, NH) of ≈98% absolute reflectance. The integration time was 6.8 msec/scan, and the number of co-adds was set to 32, whereupon the spectrum was transformed to $\log(1/R)$ and stored in a computer file. Because of a slight variation in wavelength difference between neighboring points (5.85–6.23 nm range), wavelength values were stored in addition to spectral response values. With linear interpolation between adjacent array elements, the spectrum was later adjusted to a constant wavelength spacing of 6 nm. Poor spectral response at wavelengths of <1,000 nm necessitated the truncation of the useable region to 1,002–1,704 nm (118 points total).

A computer-controlled two-axis movable stage, whose surface contained 49 (7 × 7 array) half-kernel-depth slots, was used to position each kernel with respect to the external lamp assembly that included a pickup optical 600-µm diameter single fiber. Aside from placing the long axis of each kernel at a constant direction, the positioning of the kernel within its slot was performed by random placement. This semi-random alignment approach was used for two reasons: 1) because truly automated systems will most likely be able to achieve this degree of alignment; and 2) previous research (Delwiche 2003) did not reveal a large improvement in accuracy when the rotational alignment of the kernel about its long axis was kept constant (crease down). Stage movement was staggered in time with respect to the duty cycle of the spectrometer, so that the kernels were scanned while at rest.

Procedure. All samples were stored at room ambient conditions (≈20°C, 50% rh). The kernels from each sample (5 g) were manually examined for visual scab damage. To avoid the problem of mistaking bleached but otherwise normal kernels for scab-damaged kernels, the visual analysis was primarily based on the texture of the kernel surface, with kernels having a noticeably shriveled appearance selected for the scab-damaged category. Depending on the severity of the scab in each URN sample, between 3 and 49 scab-damaged kernels were selected, with the upper number equaling the number of slots in the surface of the movable stage. From the same sample, an equal number of kernels of normal appearance were drawn. Before scanning, kernels in each sample were separately weighed to the nearest 0.01 mg. Altogether, for the URN set, 868 scab-damaged kernels and an equal number of normal kernels were weighed and scanned. Spectral scanning of all URN samples was completed before commencing the scans of the AY samples.

For the AY samples, 10 scab-damaged and 10 normal kernels were drawn from each sample. The only procedural difference with this set of samples was in the sequencing of scab-damaged and normal kernels during scanning. For this set, the kernels in each sample were scanned in an alternating pattern ($N_1S_1 \ldots N_{10}S_{10}$, where N = normal, S = scab-damaged, and the index is the kernel number), as opposed to a one-group-first pattern ($N_1 \ldots N_nS_1 \ldots S_n$, where the subscript n is the number of kernels in each category of a sample) procedure of the URN set. This change in procedure was intended to minimize the likelihood of instrument bias affecting classification predictions. Altogether, the AY set consisted of 1,790 kernels each of scab-damaged and normal types.

Repeatability. One sample from the AY set was arbitrarily selected (i.e., the first replicate of Verde from St. Paul) for repeated spectral measurement. The 10 normal and 10 scab-damaged kernels of this sample were repeatedly loaded on the movable stage, scanned, and removed from the stage a total of five times.

DON analysis. For the purpose of corroborating the presence of the mycotoxin in the visually scab-damaged and normal kernels, the repeatability sample was also used for DON analysis. The appearance of the 20 kernels of this sample was typical of that of all the samples. Digital images of these kernels under low magnification were collected. These kernels were then individually ground and analyzed for DON concentration by ELISA.

Classification modeling. Samples from the URN set were used in the development (by cross-validation) of each classification model, while samples from the AY set were reserved for testing the model. Results from a previous study indicated that the optimal classification models by linear discriminant analysis (LDA), as gauged by a high number of correct assignments and a low number of variables, was achieved with a wavelength difference $[A_{\lambda 1} - A_{\lambda 2} = \log(1/R)_{\lambda 1} - \log(1/R)_{\lambda 2}]$ and kernel mass (Delwiche 2003). Therefore, the current study placed an emphasis on this model structure, although other models (defined later) were tested. Using the procedure **Discrim** (SAS Institute Inc., Cary, NC) within a SAS Macro loop, an exhaustive search of all wavelength differences (6,903 possibilities) was performed to identify the differences that produced high average leave-one-out cross-validation accuracies. The squared distance metric for the discriminant function was based on a pooled (across-category) covariance matrix. Particular interest was given to differences formed from wavelengths that were equal to or less than the half-width of absorption bands apparent in the $\log(1/R)$ spectra. In such cases, a difference could be interpreted to represent the slope (i.e., first derivative) of the spectrum at the midpoint between the wavelengths. In so doing, classification ability becomes interpretable in terms of the spectral first derivative.

Another modeling approach included linear discriminant analysis, using the scores from a principal components analysis (PCA) of the 1,102–1,704 nm spectrum as variables. In this case, the SAS procedures **Princomp** and **Stepdisc** were used to reduce the number of spectral points from 118 wavelengths to between 1 and 15 factors, and identify the three most important PC, respectively. As detailed by Downey et al (1994), these PC are not necessarily the ones of greatest corresponding eigenvalues (PC 1, 2, …) but rather, the ones that are most beneficial in group separation. Linear discriminant models, with and without kernel mass, were evaluated by cross-validation and by application of the model to the test set. In the latter application, the SAS procedure **Scores** was first used to calculate the scores of the samples from the test set with respect to the basis of the cross-validation set PC. This sequence of steps was also used to develop a sequence of nonparametric (k-nearest-neighbor) models. Between k = 1 and 49 nearest neighbors (even numbers excluded to avoid occurrences of ties) were examined. Based on morphological and color features from digital image analysis, similar parametric and nonparametric discriminant analyses in SAS for recognition of various categories of wheat kernel damage (not including scab) were used with success by Luo et al (1999). One additional whole-spectrum approach, partial least squares (PLS) regression, was examined, due to the successful application of this approach in the single-kernel classification of red vs. white wheat (Delwiche and Massie 1996; Dowell 1998; Wang et al 1999). With this approach, the normal and scab-damaged kernels were regressed to two constant values, such that the midpoint between these values constituted the boundary between classes. The purpose of

Fig. 1. Images of normal (upper row) and visually scab-damaged (lower row) kernels. Level of DON concentration is (upper row, left to right) 0.0, 1.7, 4.9, 4.4, and 15 ppm; (lower row, left to right) 180, 14, 880, 750, and 500 ppm.

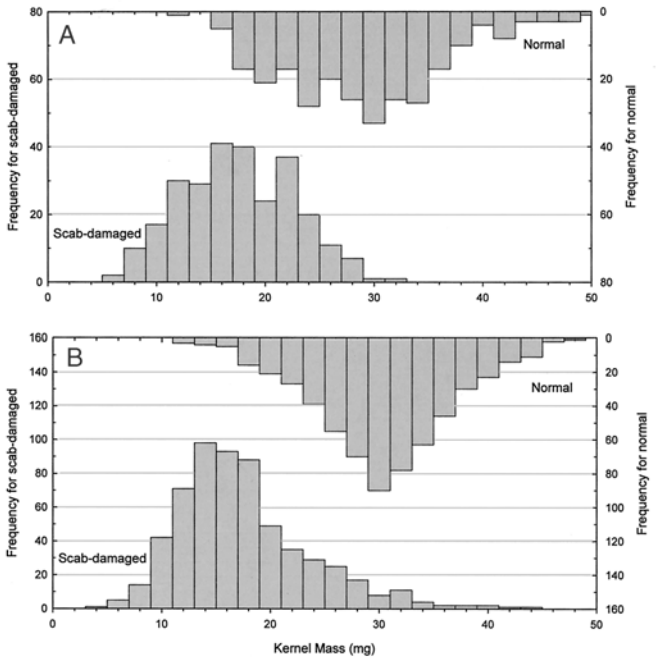

Fig. 2. Histograms of single kernel masses. **A,** URN cross-validation set (normal [n = 868], scab-damaged [n = 868]); **B,** AY test set (normal [n = 1,790] scab-damaged [n = 1,790]).

including the whole-spectrum approaches was to establish a realistic limit for the accuracies of the LDA wavelength difference models. Undoubtedly, classification accuracy is limited by the reference visual analysis procedure because it is known that *Fusarium* can be present in kernels of healthy appearance (Dexter and Nowicki 2003).

RESULTS AND DISCUSSION

A composite image of kernels that were representative of the normal and scab-damaged categories is shown in Fig. 1. Ten kernels are shown as representative of the 20 kernels that constituted one sample of the AY set, whose appearance, in turn, is representative of all the hand-selected and scanned kernels of the present study. Also included in Fig. 1 are the DON concentrations. Of the five kernels with visible scab damage, the DON concentration range was 14–880 ppm. Generally, the degree of visible scab damage coincided with the DON level. Of the five normal kernels, all but one had a DON level of <5 ppm. The remaining normal kernel, at 15 ppm, was approximately equivalent in DON level as the least affected of the five scab-damaged kernels. Compared with kernel plumpness, length and width of the kernels were much less affected by scab.

The distributions of kernel mass are separately shown by category for the URN and AY sets in Fig. 2A and B, respectively. Scab-damaged kernels seldom weighed >30 mg. Conversely, normal kernels seldom weighed <15 mg. Using mass alone on samples from the individual locations, LDA models achieved average cross-validation classification accuracies of 80.9 and 85.3% for the Crookston and St. Paul locations, with corresponding average test classification accuracies of 88.9 and 88.7% (Table I). When the two locations were combined, the resulting average classification accuracies were 83.8 and 89.3% for the cross-validation and test sets, respectively. Thus, these values stand as a basis for the development of NIR models, for which the improvement in accuracy associated with an NIR model, with or without including kernel mass, must be considered in context of the additional complexity in hardware of a scab-detection instrument. However, it is reasoned that mass-alone models would experience a lower level of accuracy with the inclusion of samples from other cultivars and geographical regions.

Plots of the spectra of normal and scab-damaged kernels, shown as averages and one-standard deviation envelopes for the URN samples, indicate that, while on average, the two categories are spectrally distinct, the degree of spectral variation within a category is sufficiently large to preclude the use of single-wavelength classification models (Fig. 3). When the first derivatives of the average spectra are formed (using an 11-point Savitzky-Golay second-order polynomial convolution), it is seen that the degree of overlap between categories becomes substantially lessened, especially in the 1,120–1,180 nm and 1,320–1,370 nm regions. Therefore, classification models that are based on wavelength differences should be superior to models that are based on single wavelengths.

Results of the average classification accuracies for all classification models examined are summarized in Table I. With the exception of the mass-alone models, the accuracies correspond to models that were developed from combining both geographical locations. Average cross-validation accuracy ranged from 82.1% (a wavelength difference, without kernel mass model) to 88.8% (a *k*-nearest-neighbor, with kernel mass model). Although the lower value in this range was indeed lower than that for a model using mass alone (83.8%), the corresponding accuracies of these models on the test (AY) set indicated that the spectrally based models, with accuracies >92% were clearly better than the mass-alone model.

TABLE I
Average Classification Accuracies for Various Discriminant Analysis Models

Model[a]	Locations Included	Average Accuracy (%)	
		Cross-Validation (n = 1,736)	Test (n = 3,580)
LDA on mass	Crookston	80.9	88.9
LDA on mass	St. Paul	85.3	88.7
LDA on mass	Both	83.8	89.3
LDA on PC 2,3,1	Both	83.1	95.7
LDA on PC 2,3,1, mass	Both	88.5	97.2
KNN (k = 21) on PC 2,3,1	Both	82.0	95.7
KNN (k = 21) on PC 2,3,1, mass	Both	88.8	97.0
PLS 9-factor	Both	87.8	92.4
LDA on $A_{1248} - A_{1140}$	Both	82.1	94.9
LDA on $A_{1248} - A_{1140}$, mass	Both	87.0	94.9
LDA on $A_{1188} - A_{1128}$	Both	82.1	94.8
LDA on $A_{1188} - A_{1128}$, mass	Both	86.9	95.1

[a] LDA, linear discriminant analysis; KNN, k-nearest-neighbor; PLS, partial least squares; PC, principal components; A_x, $\log(1/R)_{\lambda = x\ nm}$.

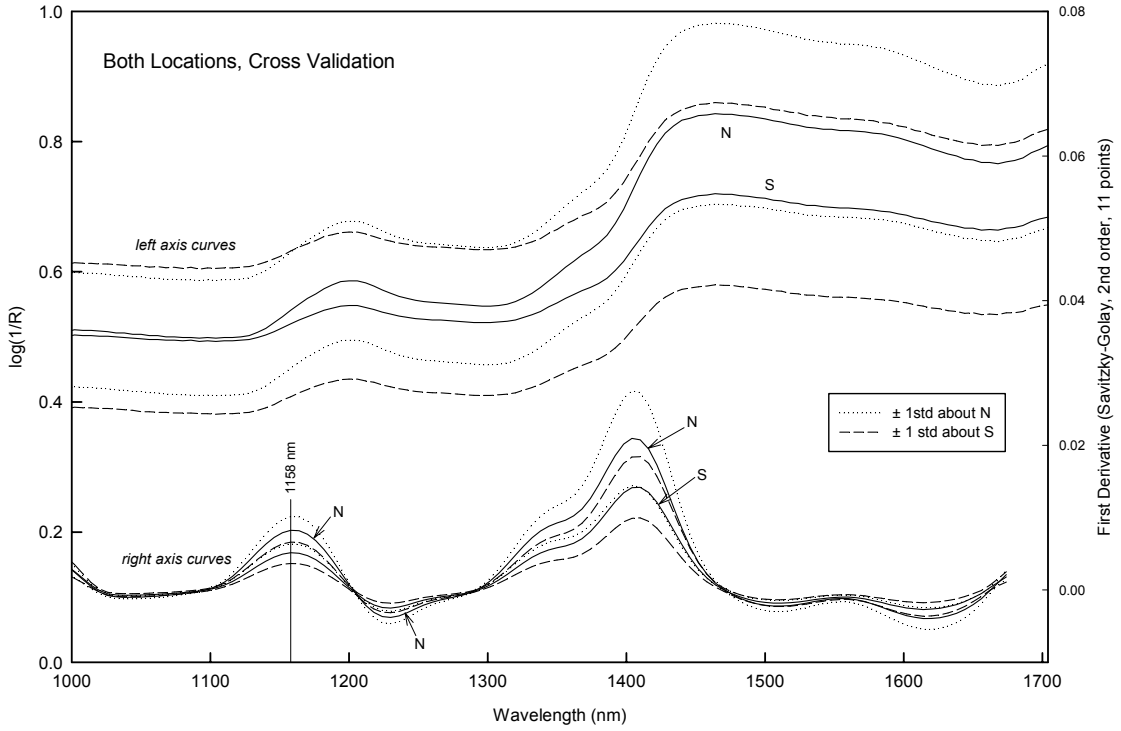

Fig. 3. Mean $\log(1/R)$ and first-derivative spectra ± 1 SD envelopes for each category of cross-validation samples (n = 868 spectra/category). N, normal; S, scab-damaged.

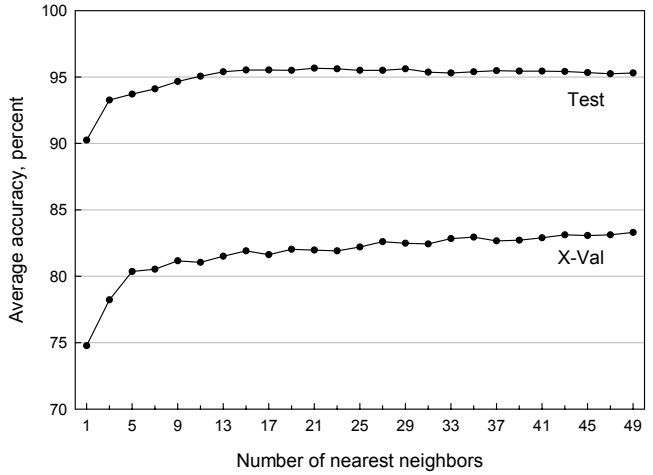

Fig. 4. Classification accuracy of a k-nearest-neighbor model of scores of the first three principal components as a function of the number of nearest neighbors during model development (X-Val) and validation (Test).

Based on test set accuracy, there were only slight differences between models that were based on PC scores and those that were based on a wavelength difference. Typically, the accuracy range was 95 and 97%. Improvement beyond this level of accuracy is probably not possible without a change in the reference method for classification (visual analysis), which undoubtedly introduced error through the categorization of a small (but unknown) fraction of scab-damaged kernels as normal kernels, and vice versa. For the k-nearest-neighbor model, the number of neighbors needed to achieve stable optimal accuracies was ≈21 (Fig. 4). The fact that the average accuracy of each classification model when applied to the test set was 3–12 percentage units higher than that of the cross-validation (URN) set indicates that the latter set had a greater degree of overlap, in both spectral and mass, between the two categories. This suggests that the URN set had greater spectral diversity, and therefore was the better of the two sets for model development.

The best wavelength difference, determined by the stepwise discriminant analysis procedure (**Stepdisc**), was ($A_{1248\ nm} - A_{1140\ nm}$), with average cross-validation and test set accuracies of 82.1 and

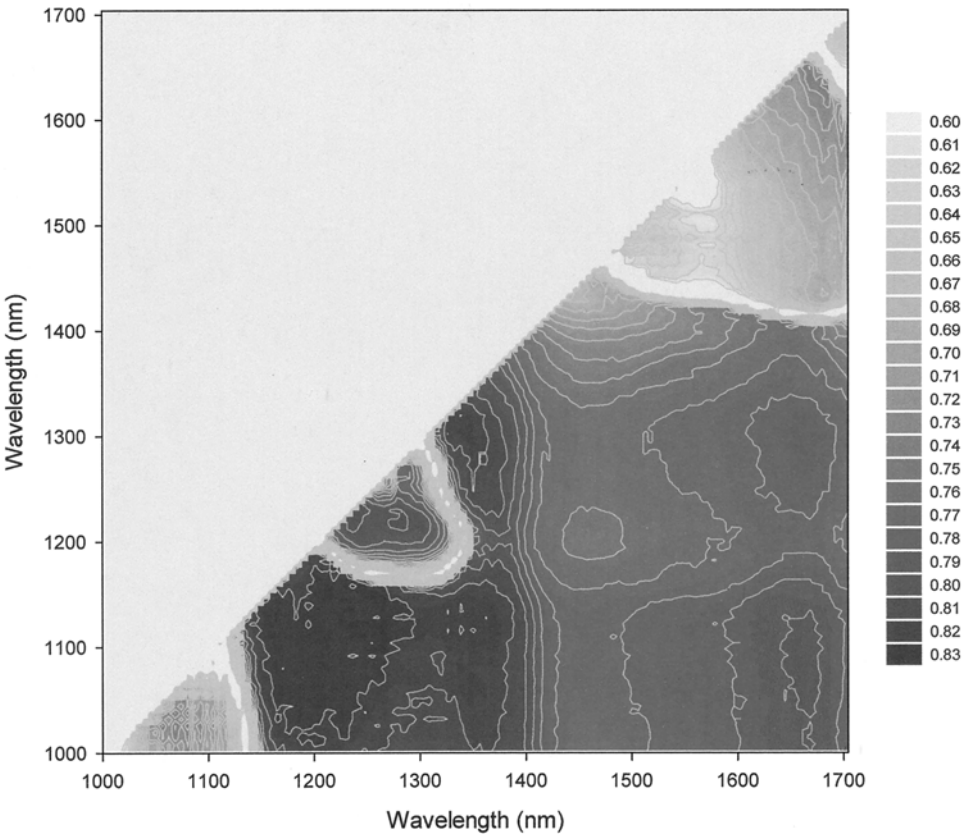

Fig. 5. Contour plot of the average cross-validation accuracy of a two-wavelength spectral difference [$\log(1/R)_{\lambda\ \text{x-axis}} - \log(1/R)_{\lambda\ \text{y-axis}}$]. Numbers in the legend refer to the average accuracies (in percent/100) of corresponding gray color levels.

TABLE II
Classification Results for Linear Discriminant Analysis Model Utilizing [$\log(1/R)_{\lambda = 1188\ \text{nm}} - \log(1/R)_{\lambda = 1128\ \text{nm}}$] With and Without Kernel Mass

	Number of Kernels Assigned to Category[a]					
	Cross-Validation Set			Test Set		
Actual Category	Scab	Normal	Total	Scab	Normal	Total
Without mass						
Scab	**744 (85.7)**	124 (14.3)	868	**1,745 (97.0)**	45 (2.5)	1,790
Normal	186 (21.4)	**682 (78.6)**	868	143 (8.0)	**1,647 (92.0)**	1,790
Total	930 (53.6)	806 (46.4)	1,736	1,888 (52.7)	1,692 (47.3)	3,580
With mass						
Scab	**767 (88.4)**	101 (11.6)	868	**1,684 (94.1)**	106 (5.9)	1,790
Normal	127 (14.6)	**741 (85.4)**	868	68 (3.8)	**1,722 (96.2)**	1,790
Total	894 (51.5)	842 (48.5)	1,736	1,752 (48.9)	1,828 (51.1)	3,580

[a] Diagonal values, in bold, represent correct assignments. Percent of total listed in parentheses.

94.9%, respectively, being nearly equivalent to the corresponding accuracies of the *k*-nearest-neighbor model (82.0 and 95.7%). Many other wavelength differences produced cross-validation accuracies that were within 0.5 percentage units of the optimal difference. To determine the existence of any trends in the selection of wavelength differences, a contour plot of the overall average cross-validation accuracy was produced (Fig. 5) where the axes represent the wavelengths used in forming the differences, and the degree of grayness represents accuracy (darker = more accurate). The near-white contour regions of low accuracy that appear as circuitous loops near x = 1,150 nm (y = 1,000–1,100 nm), x = 1,200–1,360 nm (y = 1,170–1,300 nm), and x = 1,500–1,700 nm (y = 1,400–1,670 nm) correspond to wavelength pairs in which the spectral absorption values were equal within each pair, such as on opposite sides of a broad absorption band. Evident from this plot is the greater importance of the lower end of the 1,000–1,700 nm scanned region, for both terms in a difference expression. Specifically, for the difference ($A_x - A_y$), the optimal values for x were in the 1,150–1,300 nm region, while the optimal values for y were in the 1,000–1,150 nm region. Combined, these regions define the broad absorption band centered near 1,200 nm, which is attributed to the second overtone of CH stretch from carbohydrates (Osborne and Fearn 1986). The left (short wavelength) side of this absorption band, specifically between 1,130–1,190 nm, appeared to be a very stable region for defining a difference that could be used in classifying normal and scab-damaged kernels. Recalling that a difference in neighboring values of a mathematical function represents an approximation to the instantaneous slope or first derivative of the function, it is seen that the 1130–1190 nm region captures the wavelength (1,158 nm) where the 1st derivative encounters a local maximum (Fig. 3). Thus, wavelengths that are centered near this local maximum are well suited to produce stable high classification accuracies. Two wavelengths, 1,128 and 1,188 nm, were selected for classification analysis because they mark the beginning and ending points of the left side of the 1,200 nm absorption band and are equidistant from 1,158 nm.

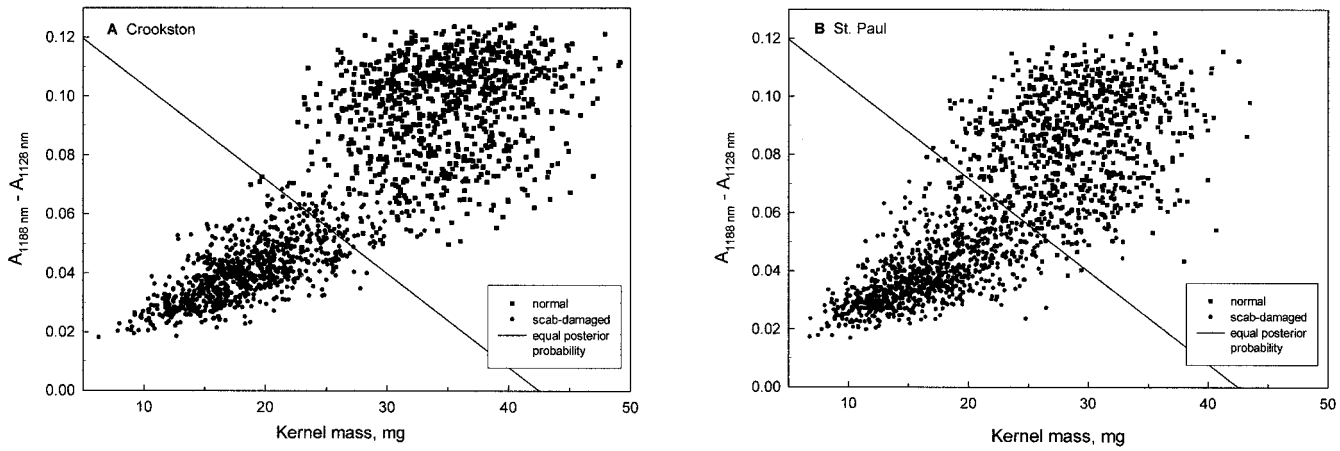

Fig. 6. Two-wavelength spectral difference [$\log(1/R)_{\lambda\ 1188\ nm} - \log(1/R)_{\lambda\ 1128\ nm}$] vs. kernel mass of the test set samples. **A,** Crookston location (normal [n = 890], scab-damaged [n = 890]); **B,** St. Paul location (normal [n = 900], scab-damaged [n = 900]). Boundary line between categories determined by linear discriminant analysis on cross-validation sample set (both locations combined) included on each graph.

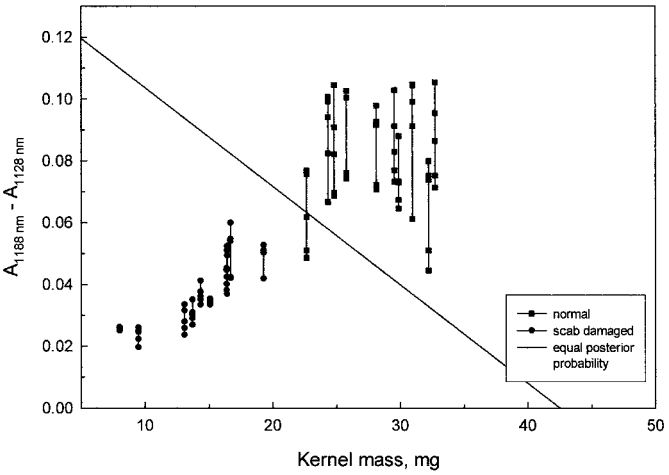

Fig. 7. Repeatability readings of [$\log(1/R)_{\lambda\ 1188\ nm} - \log(1/R)_{\lambda\ 1128\ nm}$] and kernel mass. Each kernel from one sample (10 normal, 10 scab-damaged) of the St. Paul AY set was repeatedly loaded and scanned five times.

The ($A_{1188\ nm} - A_{1128\ nm}$) without-mass model achieved an overall cross-validation accuracy of 82.1% (Table I). With mass, this rate reached 86.9%. When applied to the test set, the two models achieved overall accuracies of 94.8 and 95.1%, respectively. For either model, the cross-validation and test accuracies were essentially equivalent (±0.2%) to the corresponding accuracies of the SAS best difference ($A_{1248\ nm} - A_{1140\ nm}$), with- and without-mass, model accuracies. Identified by category, misclassifications during cross-validation occurred more frequently for normal kernels identified as scab-damaged, as opposed to scab kernels identified as normal, regardless of whether the model included mass (Table II). During application to the test set, the models were not consistent in terms of which category had the greater number of misclassifications. Rather, misclassification occurred at a greater rate with normal kernels when mass was not included in the model and a lesser rate when mass was included. Plots of ($A_{1188\ nm} - A_{1128\ nm}$) vs. kernel mass for the test set are shown in Fig. 6A (Crookston) and Fig. 6B (St. Paul). Within each graph, misclassified normal kernels are those lying to the left of the boundary that marks the line where posterior probability from linear discriminant analysis is equal between categories. Likewise, misclassified scab-damaged kernels are those to the right of the boundary line. Similar analysis in which a quadratic discriminant function was used (covariance matrices of the two groups are not pooled) did not improve cross-validation and test set accuracies (results not shown).

Repeatability of wavelength difference model. When 20 kernels (10 normal, 10 scab-damaged) of one AY set sample were repeatedly loaded and scanned five times, the application of the ($A_{1188\ nm} - A_{1128\ nm}$) with-kernel-mass model resulted in correct classification in all but three of 100 applications (Fig. 7). The three misclassifications occurred on the same kernel (center image in the top row of Fig. 1), which, of the 10 normal kernels examined had the smallest mass from that category. Still, this kernel was greater in mass than the heaviest of the scab-damaged kernels, indicating that, in this case, mass alone could have been used as the classifier. As the magnitude of ($A_{1188\ nm} - A_{1128\ nm}$) increased and as kernel mass increased, so did the variability of this spectral difference. Therefore, it is logical that the kernels most susceptible to misclassification are those of intermediate mass and spectral difference.

Using both light and electron microscopy, Bechtel et al (1985) observed that *Fusarium*-damaged kernels had degraded starch granules and a general dissolution of the starchy endosperm walls and parts of the starchy endosperm, as well as an invasion of the fungus into the storage protein matrix. The fungi's preference for endosperm instead of germ, as stated in Bechtel et al (1985), is thought to be the reason for the high classification accuracies associated with the 1,200 nm carbohydrate band. Because it was beyond the scope of this study to examine other wheat-damaging molds, it is not possible to definitively state the specificity of the broad carbohydrate absorption band at 1,200 nm toward molds other than *Fusarium*. However, recent work by Pearson et al (2004) on detection of *Aspergillus flavus* on yellow corn kernels for two-wavelength high-speed sorting has demonstrated the preference of 1,200 nm in combination with absorbance at a smaller wavelength (750 nm, in which a wavelength at <1,000 nm is mandated because of sorter detector element constraints). These wavelengths were also suitable at the detection of *F. verticillioides*, a fungus responsible for the production of fumonisins in corn. Therefore, it is postulated that the 1,200 nm band, in general, is sensitive for detection of kernels afflicted with nonstorage fungi.

SUMMARY AND CONCLUSIONS

Identification of scab-damaged wheat kernels is most effective when single kernel NIR reflectance is combined with kernel mass. For scanning, the kernels may be oriented in just a semi-random basis, in which the rotational angle about a kernel's long axis is arbitrary. Simple classification model structures such as linear discriminant analysis (LDA) operating on the difference of spectral absorption at two wavelengths and mass at 95% test set average accuracy performed nearly as well as whole spectrum parametric (LDA on principal component scores) or nonpara-

metric (*k*-nearest-neighbor) models. The best wavelengths to use in a spectral difference model were located in the sloped region that approaches the broad absorption band at ≈1,200 nm. Essentially, the left-side (shorter wavelength) slope of this absorption band can be used to discriminate between normal and scab-damaged kernels. While the classification accuracies may not be sufficient for fully automated official inspection, it is thought that a two-wavelength system could have application in high-speed commercial sorting and for use as a breeder's assistant. Quantification of the reduction in levels of DON that can be achieved through sorting and the examination of wavelengths at <1,000 nm are the subjects of future research.

ACKNOWLEDGMENTS

We wish to thank J. Anderson (Univ. of Minnesota) for the wheat samples, B. Stetzler (ARS, Beltsville) for spectral data collection, P. Hart (Michigan State Univ.) for DON analysis, and A. Collins (ARS, Beltsville) for the production of the magnified images.

LITERATURE CITED

Abramson, D., Clear, R. M., Usleber, E., Gessler, R., Nowicki, T. W., and Märtlbauer, E. 1998. *Fusarium* species and 8-keto-trichothecene mycotoxins in Manitoba barley. Cereal Chem. 75:137-141.

Bai, G.-H., and Shaner, G. 1994. Scab of wheat: Prospects for control. Plant Dis. 78:760-766.

Bechtel, D. B., Kaleikau, L. A., Gaines, R. L., and Seitz, L. M. 1985. The effects of *Fusarium graminearum* infectin on wheat kernels. Cereal Chem. 62:191-197.

Casale, W. L., Pestka, J. J., and Hart, L. P. 1988. Enzyme-linked immunosorbent assay employing monoclonal antibody specific for deoxynivalenol (vomitoxin) and several analogues. J. Agric. Food Chem. 35:663-668.

Chang, H. L., DeVries, J. W., Larson, P. A., and Patel, H. H. 1984. Rapid determination of deoxynivalenol (vomitoxin) by liquid chromatography using modified Romer column cleanup. J. AOAC 67:52-54.

Cunfer, B. M. 1987. Bacterial and fungal blights of the foliage and heads of wheat. Pages 528-541 in: Wheat and Wheat Improvement, 2nd Ed. E. G. Heyne, ed. Am. Soc. Agron.: Madison, WI.

Delwiche, S. R. 2003. Classification of scab- and other mold-damaged wheat kernels by near-infrared reflectance spectroscopy. Trans. ASAE 46:731-738.

Delwiche, S. R., and Massie, D. R. 1996. Classification of wheat by visible and near-infrared reflectance spectroscopy. Cereal Chem. 73:399-405.

Dexter, J. E., and Nowicki, T. W. 2003. Safety assurance and quality assurance issues associated with Fusarium head blight in wheat. Pages 420-460 in: Fusarium Head Blight of Wheat and Barley. K. J. Leonard and W. R. Bushnell, eds. APS: St. Paul, MN.

Dexter, J. E., Clear, R. M., and Preston, K. R. 1996. Fusarium head blight: Effect on the milling and baking of some Canadian wheats. Cereal Chem. 73:695-701.

Dowell, F. E. 1998. Automated color classification of single wheat kernels using visible and near-infrared reflectance. Cereal Chem. 75:142-144.

Dowell, F. E., Ram, M. S., and Seitz, L. M. 1999. Predicting scab, vomitoxin, and ergosterol in single wheat kernels using near-infrared spectroscopy. Cereal Chem. 76:573-576.

Downey, G., Boussion, J., and Beauchene, D. 1994. Authentication of whole and ground coffee beans by near-infrared reflectance spectroscopy. J. Near Infrared Spectrosc. 2:85-92.

Fernandez, C., Stack, M. E., and Musser, S. M. 1994. Determination of deoxynivalenol in 1991 U.S. winter and spring wheat by high-performance thin-layer chromatography. J. AOAC Int. 77:628-630.

Luo, X., Jayas, D. S., and Symons, S. J. 1999. Identification of damaged kernels in wheat using a colour machine vision system. J. Cereal Sci. 30:49-59.

Osborne, B. G., and Fearn, T. 1986. Near-Infrared Spectroscopy in Food Analysis. Wiley and Sons: New York

Pearson, T. C., Wicklow, D. T., and Pasikatan, M. C. 2004. Reduction of aflatoxin and fumonisin contamination in yellow corn by high-speed dual wavelength sorting. Cereal Chem. 81:490-498.

Pettersson, H., and Åberg, L. 2003. Near-infrared spectroscopy for determination of mycotoxins in cereals. Food Control 14:229-232.

Rajaklyä, E., Laasasenaho, K., and Sakkers, P. J. D. 1987. Determination of mycotoxins in grain by high-performance liquid chromatography and thermospray liquid chromatography-mass spectrometry. J. Chromatogr. 384:391-402.

Ruan, R., Ning, S., Song, A., Ning, A., Jones, R., and Chen, P. 1998. Estimation of *Fusarium* scab in wheat using machine vision and a neural network. Cereal Chem. 75:455-459.

Scott, P. M., Kanhere, S. R., and Tarter, E. J. 1986. Determination of nivalenol and deoxynivalenol in cereals by electron-capture gas chromatography. J. AOAC 69:889-893.

Scott, P. M., Lau, P.-Y., and Kanhere S. R. 1981. Gas chromatography with electron capture and mass spectrometric detection of deoxynivalenol in wheat and other grains. J. AOAC 64:1364-1371.

Tacke, B. K. and Casper, H. H. 1996. Determination of deoxynivalenol in wheat, barley, and malt by column cleanup and gas chromatography with electron capture detection. J. AOAC Int. 79:472-475.

Teich, A. H., Shugar, L., and Smid, A. 1987. Soft white winter wheat cultivar field-resistance to scab and deoxynivalenol accumulation. Cereal Res. Commun. 15:109-114.

Terhune, S. J., Nguyen, N. V., Baxter, J. A., Pryde, D. H., and Qureshi, S. A. 1984. Improved gas chromatographic method for quantitation of deoxynivalenol in wheat, corn, and feed. J. Assoc. Off. Anal. Chem. 67:1102-1104.

Tkachuk, R., Dexter, J. E., Tipples, K. H., and Nowicki, T. W. 1991. Removal by specific gravity table of tombstone kernels and associated trichothecenes from wheat infected with Fusarium head blight. Cereal Chem. 68:428-431.

Trenholm, H. L., Warner, R. M., and Prelusky, D. B. 1985. Assessment of extraction procedures in the analysis of naturally contaminated grain products for deoxynivalenol (vomitoxin). J. AOAC 68:645-649.

Truckness, M. W., Nesheim, S., and Eppley, R. M. 1984. Thin layer chromatographic determination of deoxynivalenol in wheat and corn. J. Assoc. Anal. Chem. 67:40-43.

USDA-GIPSA. 1997. Wheat. Chapter 13 in: Grain Inspection Handbook, Book II (release date 6/1/97). Grain Inspection, Packers and Stockyards Administration. USDA: Washington, DC.

Usleber, E., Märtlbauer, E., Dietrich, R., and Terplan, G. 1991. Direct enzyme-linked immunosorbent assays for the detection of the 8-ketotrichothecene mycotoxins deoxynivalenol, 3-acetyldeoxynivalenol, and 15-acetyldeoxynivalenol in buffer solutions. J. Agric. Food Chem. 39:2091-2095.

Usleber, E., Schneider, E., Märtlbauer, E., and Terplan, G. 1993. Two formats of enzyme immunoassay for 15-acetyldeoxynivalenol applied to wheat. J. Agric. Food Chem. 41:2019-2023.

Wang, D., Dowell, F., and Lacey, R. 1999. Single wheat kernel color classification by using near-infrared reflectance spectra. Cereal Chem. 76:30-33.

Ware, G. M., Carman, A., Francis, O., and Kuan, S. 1984. Gas chromatographic determination of deoxynivalenol in wheat with electron capture detection. J. AOAC 67:731-734.

Williams, P. C. 1997. Recent advances in near-infrared applications for the agriculture and food industries. Pages 109-128 in: Proc. Int. Wheat Quality Conf. J. L. Steele and O. K. Chung, eds. Grain Industry Alliance: Manhattan, KS.

[Received October 29, 2003. Accepted May 5, 2004.]